Chapter 6

EPOLLS Database of Lateral Spreads

6.1. Introduction.

As pointed out by Glaser (1993; 1994), assembling a database of field case studies is a laborious, yet critical, task in the development of an empirical model for lateral spreading. The EPOLLS model was derived from the database described in this chapter and tabulated in Appendix A. Data were compiled on 78 lateral spreads from 16 earthquakes in western North America and eastern Asia, mostly in California, Alaska, and Japan. These case studies are described, in general terms, in the next section. Many of these lateral spreads are also in the database compiled by Bartlett and Youd (1992b), although case studies from eight additional earthquakes were included in the EPOLLS database. The site investigation reports and other reference materials used in assembling the EPOLLS database are listed in Appendix B.

Only lateral spreads conforming to the definition adopted in Sections 3.1 and 5.1 were compiled in the EPOLLS database. "Lateral spreads" more correctly associated with the slumping of embankments or the outward rotation of retaining walls were not compiled in the EPOLLS database. For example, port facilities constructed by loose filling behind quay walls are often heavily damaged by increased active earth pressures that result from liquefaction in the backfill. The resulting lateral movements in the zone immediately behind these walls do not constitute a lateral spread suitable for the EPOLLS database. Moreover, sites subjected to lateral spreading over a fairly large area, but with massive earth-retaining structures (concrete caissons, cellular cofferdams, rock-fill dikes) along the toe are not included in the EPOLLS database. On the other hand, several sites in the EPOLLS database have relatively flexible sheet pile walls along the toe of the slide. In these cases, the flexible wall was judged to have a negligible effect on the deformation of the comparably large sliding mass of the lateral spread. Statistical analyses during development of the EPOLLS model confirmed this hypothesis by showing that the deformation of these sites were not substantially different than similar sites without a wall.

To be included in the EPOLLS database, a post-earthquake site investigation must specifically link lateral spreading to soil liquefaction in a subsurface deposit. Evidence for liquefaction includes surface manifestations such as sand boils or the analysis of in situ penetration tests that confirm liquefaction as the cause of the ground failure.

Having selected the EPOLLS case studies, appropriate parameters were then chosen for compilation in the database. These variables are grouped into four categories:

(1) *Seismological parameters* include the earthquake magnitude and source distance, as well as the intensity of shaking at the case study site.
(2) *Geometrical parameters* indicate the area and shape of the surface of the lateral spread.
(3) *Topographical parameters* include the surface slope and free face height.
(4) *Geotechnical parameters* encompass all variables derived from soil borings such as the thickness of liquefied soil, penetration resistance, and grain size characteristics.

The parameters in each of these categories are discussed in Sections 6.3 through 6.7.

The variables chosen for the EPOLLS database reflect the physical mechanics of liquefaction and lateral spreading discussed in Chapter 3. However, only parameters that can be defined with reasonable accuracy and ease for a lateral spread in the field were chosen for the EPOLLS database. For example, it is recognized that the shear resistance of the liquefied soil deposit plays a role in controlling the magnitude of deformations in a lateral spread. However, the residual shear strength of a liquefied natural soil is difficult to determine from laboratory tests and is almost never known with confidence in the study of lateral spreads. Hence, in the EPOLLS database, the shear strength of the liquefied soil is represented only indirectly with the in situ penetration resistance. No parameters from laboratory strength tests were compiled in the EPOLLS database.

The amount of information available varies considerably among the different EPOLLS case studies. At a minimum, measured displacements of the ground surface must be available for a lateral spread to be included in the database. Many of the EPOLLS case studies are thoroughly documented, while little quantitative data are available for other case studies. Since the geologic source of nearly all large earthquakes in this century have been established, the seismological parameters are available for every EPOLLS case study. Information on the surface topography is available for most of the case studies, while soil borings are available for only about three quarters of the EPOLLS database. However, many of the EPOLLS parameters could not be defined for all case studies. These "missing values", which require special consideration during model development, appear as blanks in the database tabulation in Appendix A.

6.2. Overview of Case Studies.

1906 San Francisco, California, Earthquake

Four case studies of lateral spreading resulting from this earthquake are included in the EPOLLS database. Two of these case studies (Slide Nos. 1 and 2) are within the city of San Francisco, in formerly low-lying areas filled with loose soils during early development of the city. Slide No. 3 damaged a bridge across the Salinas River near Monterey Bay, while Slide No. 4 damaged a bridge near the southern end of San Francisco Bay. Displacements at these sites were

determined mostly from contemporary reports of earthquake damage. Slide No. 2 is shown in Figure 6.1.

1923 Kanto, Japan, Earthquake

This infamous earthquake caused tremendous destruction and loss of life in the Tokyo area. Lateral spreading occurred along the Furu-Tone River in the city of Kasukabe, north of Tokyo. Displacements for one EPOLLS case study were measured by the lateral offset of a city street.

1948 Fukui, Japan, Earthquake

Four EPOLLS case studies were compiled from investigations of liquefaction damage in this earthquake. These lateral spreads occurred on both sides of the Yoshino River, a tributary of the Kuzuryu River, near the west coast of the island of Honshu. Surface displacements were measured from aerial photographs of the area, taken before and after the earthquake. Two case studies (Slide Nos. 8 and 9) are depicted in Figure 6.2.

1964 Prince William Sound, Alaska, Earthquake

This extremely large-magnitude earthquake caused extensive damage across southern Alaska. Fifteen lateral spread case studies were compiled for the EPOLLS database. In each case, displacements were determined from the offset of bridge piers along the Alaska Railroad, the Seward-Anchorage Highway, and the Glenn Highway. In some of these cases, displacements were estimated many years later by measuring how far the rail bearing plates were moved during repairs after the earthquake. Good maps showing cracks in the ground surface, useful in delineating the area and direction of sliding, are available for many of these sites. An example of these maps is shown in Figure 6.3. Here, three lateral spreads (Slide Nos. 10 through 12) damaged railroad and highway bridges crossing the Resurrection River.

1964 Niigata, Japan, Earthquake

Extensive liquefaction-induced ground failures occurred throughout the west-coast city of Niigata. Fourteen lateral spreads were identified for the EPOLLS database: eleven of these slides were in Niigata along the banks of the Shinano River, one was on the west bank of the Agano River, and two cases were along the much smaller Tsusen River. Slide Nos. 31 and 32, located just east of the Shinano River, are shown in Figure 6.4 and Slide Nos. 37 and 38, along the Tsusen River, are shown in Figure 6.5. In all fourteen case studies, displacements of the ground surface were measured from aerial photographs taken before and after the earthquake. The lateral spreads in Niigata, which are some of the best-documented case studies in the EPOLLS database, involved very large surface displacements.

1971 San Fernando, California, Earthquake

Two lateral spreads were identified in San Fernando, California, which is at the north end of the Los Angeles metropolitan area. Slide No. 40 involved the lateral deformation of a fill

underlying the Joseph Jensen Water Filtration Plant. Deformations in this area were determined from both aerial photographs and optical surveys, with adjustments for tectonic movements in the area. Slide No. 41, shown in Figure 6.6, extends from the San Fernando Valley Juvenile Hall facility to the Upper Van Norman Reservoir. Here, displacements were measured from aerial photographs, optical surveys, and the offsets of streets.

1976 Guatemala Earthquake

EPOLLS Slide No. 42 occurred in the Villalobos River Delta on the shore of Lake Amatitlan in Guatemala. Maximum displacements were estimated from the cumulative offsets measured across fissures in the ground surface.

1979 Imperial Valley, California, Earthquake

Occurring south of the Salton Sea in the Imperial Valley of southern California, two lateral spreads were included in the EPOLLS database. Slide No. 43 is a well-documented lateral spread of fairly small area in which displacements were determined mostly from the offset of a small irrigation canal. Very small displacements, indicative of the reported surface cracking in the area, were assumed for Slide No. 44.

1983 Nihonkai-Chubu, Japan, Earthquake

Five well-documented case studies were obtained with surface displacements determined from the analysis of aerial photographs. These lateral spreads all occurred in the west coast city of Noshiro, Japan. Slide Nos. 45 through 48 are shown in Figure 6.7. The surface deformation in Slide No. 49, with 187 measured displacement vectors, is the most extensively documented in the EPOLLS database.

1983 Borah Peak, Idaho, Earthquake

Two lateral spreads underlain by gravelly soils were studied following this earthquake in south-central Idaho. Because of the high gravel content in the liquefiable soils at both sites, Standard Penetration Tests (SPTs) are unreliable. Hence, the geotechnical EPOLLS parameters for these sites were derived from Becker Penetration Test logs that were converted to equivalent SPT blowcounts (see Section 7.2). Since the high gravel content in the underlying soil might have a significant impact on lateral spreading, these two case studies were investigated as possible outliers during development of the EPOLLS model. However, statistical analysis indicated that the deformation of these two sites was not outside the trend of the other case studies in the database.

1987 Superstition Hills, California, Earthquake

Only one case study was recorded from this earthquake. The lateral spread developed at the Wildlife Liquefaction Array located along the Alamo River, southeast of the Salton Sea in southern California. This site has been instrumented by the U.S. Geological Survey to record the onset of soil liquefaction during an earthquake.

1989 Loma Prieta, California, Earthquake

From ground failures caused by this earthquake, five case studies were compiled. This earthquake caused extensive damage in the San Francisco metropolitan area. In two areas in the city of San Francisco, where lateral spreading occurred in the 1906 earthquake, evidence of soil liquefaction was observed again in 1989. However, no consistent pattern of horizontal movement was observed in 1989. Thus, these two sites were included in the EPOLLS database with a zero average horizontal displacement. Another EPOLLS case study (Slide No. 55) was a lateral spread that developed at Moss Landing Spit on the eastern shore of Monterey Bay. Two other EPOLLS case studies, Slide Nos. 56 and 57, are lateral spreads that developed in the agricultural fields along the Pajaro River just east of Watsonville, California.

1990 Luzon, Philippines, Earthquake

Four lateral spreads, occurring along the Pantal River in the city of Dagupan, Philippines, were included in the database. Dagupan is located north of Manila on the west coast of the island of Luzon. Displacements at these four sites were estimated from damage to structures in the area.

1991 Telire-Limon, Costa Rica, Earthquake

Damages to one highway bridge and four railroad bridges were used to estimate displacements for five case studies from this earthquake. Only minimal information is available from these sites.

1993 Hokkaido Nansei-oki, Japan, Earthquake

In the floodplain of the Shiribeshi-toshibetsu River, near the southwest coast of the island of Hokkaido, nine lateral spreads were documented. Displacements, surface cracks, and sand boils were mapped from aerial photographs of the area. Slide Nos. 115 through 117 are shown in Figure 6.8.

1994 Northridge, California, Earthquake

This earthquake caused damages over roughly the same area as the 1971 San Fernando earthquake. At the San Fernando Valley Juvenile Hall site (Slide No. 118), much smaller displacements were reported in 1994 than for the same site in 1971. The other case studies obtained from this earthquake were not extensively documented.

1995 Hyogoken-Nanbu, Japan, Earthquake

This earthquake caused massive liquefaction damage in the port city of Kobe, Japan, located on the western side of Osaka Bay. However, no case studies of lateral spreading have been reported that would be suitable for inclusion in the EPOLLS database. Most of the liquefaction damage in Kobe occurred along the waterfront and on man-made islands in the city. These areas were typically constructed by filling behind large, sand-filled, concrete caisson structures. While extensive lateral deformation of the ground in Kobe resulted from soil liquefaction, none of these failures appear to have occurred in the absence of a massive earth-

retaining structure. Therefore, no case studies from this earthquake are in the EPOLLS database.

6.3. Horizontal and Vertical Displacements.

The average, standard deviation, and maximum measured horizontal and vertical displacements are compiled in the EPOLLS database. These six values for the surface deformation in a lateral spread are identified with:

- *Avg_Horz* is the average horizontal displacement,
- *StD_Horz* is the standard deviation of the horizontal displacements,
- *Max_Horz* is the maximum observed horizontal displacement,
- *Avg_Vert* is the average vertical displacement,
- *StD_Vert* is the standard deviation of the vertical displacements,
- *Max_Vert* is the maximum observed vertical displacement.

Settlements are recorded as positive vertical displacements, while uplift or heaving is taken as a negative vertical displacement.

The above values were computed using all of the measured displacement magnitudes available in the published site investigation reports. The numbers of horizontal and vertical displacement vectors measured on each lateral spread are listed in the EPOLLS database. However, in about one-third of the case studies, few displacement magnitudes were measured. In these cases, the average or maximum displacement was approximated from whatever information was available. For example, in a post-earthquake damage report, the average or maximum movement might have been approximated by an observer at the site. In some cases, the compression of a bridge was used to estimate the average deformation, with one half of the movement attributed to lateral spreads on each side of the stream.

When horizontal and vertical displacements were directly measured in the investigations of the EPOLLS case studies, movements were determined in one of four ways:

(1) Offsets in streets, curbs, sidewalks, fences, lined drainage channels, etc. that cross a lateral spread, as well as the compression or extension of bridges and pipelines.
(2) Cumulative offsets across fissures in the ground surface, measured along traverse lines.
(3) Optical surveys used to locate reference points, with displacements determined by comparing positions before and after an earthquake.
(4) Analysis of aerial photographs, taken before and after an earthquake, showing the movement of selected reference points.

For the optical surveys and aerial photographic analysis, reference points included utility poles, fence posts, manhole covers, corners of drainage channels, corners on small buildings, and other similar points.

Reference points for measuring displacements are assumed to have moved with the

surrounding ground without imparting a significant restraint to the local deformation. While this may not be true in the strictest sense, the reported measurements are believed to give a reasonable indication of the free-field, horizontal, surface deformations. However, because of possible loss of bearing capacity, some reference points may have settled more than the surrounding ground surface. Other reference structures may have been subjected to tilting, or even upward floating, which would also affect the measured vertical displacement. In general, the reported vertical displacements are considered to be less reliable than the horizontal displacements as measures of the free-field deformation on a lateral spread.

Regardless of the method used to determine surface displacements, some error is associated with these measurements. However, it is reasonable to assume that these errors are random. Moreover, while the displacement at any given point may not be measured with great accuracy, the average displacement computed from measurements at multiple locations should be closer to the true average displacement of a lateral spread. Consequently, the average and standard deviation of the surface displacements are known with greater confidence than the displacement at any single location. As more displacement vectors are measured, the average and standard deviation are known with greater accuracy because these values are less sensitive to random errors in the individual measurements. On the other hand, the maximum measured displacement is a single value known with much less confidence. In addition to possible measurement error, the largest observed displacement might be significantly less than the true maximum deformation, which might have occurred in an area where displacements were not determined.

In the EPOLLS case studies, displacements at specific locations are measured with the greatest precision when lateral offsets in streets, etc. are measured. The magnitude of these displacements are probably accurate to within a few centimeters. On the other hand, the precision of the individual displacement magnitudes determined from aerial photographs is considerably less. For example, the horizontal displacements measured in Niigata and Noshiro, Japan, are believed to be accurate to within only ± 72 cm and ± 13 cm, respectively. However, the analysis of aerial photographs usually yields many more measured displacement vectors across the surface area of the lateral spread. For this reason, the values of average, maximum, and standard deviation of the displacements are often known with greater confidence when determined from aerial photographs. Overall, it is difficult to quantitatively express the accuracy associated with the displacements compiled in the EPOLLS database.

Histograms of the average displacements compiled in the EPOLLS database are shown in Figure 6.9. These plots give a picture of the dispersion of horizontal and vertical displacement magnitudes in the database. As can be seen in Figure 6.9a, the average horizontal displacement is less than 1.6 m in most of the EPOLLS case studies. On the other hand, nine lateral spreads had average horizontal displacements exceeding 3.0 m; all of these case studies occurred in 1964 in Niigata, Japan. While the Niigata case studies involved very large displacements, most of the

EPOLLS case studies experienced small to moderate horizontal displacements. In addition, the average settlement in most of the EPOLLS case studies is less than 0.7 m, as indicated by the histogram in Figure 6.9b. Hence, these histograms suggest that smaller and less damaging lateral spreads are probably not severely under-represented in the assembled database.

6.4. Seismological Parameters.

The EPOLLS seismological parameters represent the size and distance to the seismic source, as well as the intensity of shaking at the site of the lateral spread. The seismological parameters are defined here and listed in Table A.2 of Appendix A.

Parameter: *EQ_Mw* = moment magnitude of the earthquake.

Because it gives a more reliable measure of earthquake size, the moment magnitude scale is preferred by many seismologists (Bolt 1993). As defined by Kanamori (1978), the moment magnitude (M_w) is computed with:

$$M_w = \frac{\log M_o}{1.5} - 10.7 \qquad (6.1)$$

The seismic moment (M_o, in dyne-cm = 10^{-7} N-m) is a measure of the work done by the fault rupture. As explained in Chapter 7, the moment magnitude is used in the evaluation of liquefaction resistance.

Parameter: *EQ_Ms* = surface-wave magnitude of the earthquake.

The surface-wave magnitude (M_s) is an empirical measure commonly used to describe the size of shallow, strong earthquakes. This magnitude scale is based on the largest measured amplitude of the surface wave with a period of about 20 seconds (Bolt 1993).

Parameter: *Focal_Depth* = focal depth of the earthquake (kilometers).

The focal depth is the depth of the earthquake hypocenter below the surface of the earth, as illustrated in Figure 6.10.

Parameter: *Epict_Dist* = epicentral distance to the earthquake (kilometers).

The epicentral distance is measured along the earth's surface from the lateral spread to the epicenter of the earthquake (surface projection of the hypocenter), as illustrated in Figure 6.10.

Parameter: *Hypoc_Dist* = hypocentral distance to the earthquake (kilometers).

The hypocentral distance is the shortest distance from the lateral spread to the earthquake hypocenter (location where the fault rupture commences) as shown in Figure 6.10. For sites subject to soil liquefaction, the epicentral distance is small enough to neglect the earth's

curvature. The hypocentral distance can then be computed from the focal depth and epicentral distance with:

$$Hypoc\_Dist = \sqrt{Epict\_Dist^2 + Focal\_Depth^2} \qquad (6.2)$$

Parameter: *Fault_Dist* = shortest horizontal distance to the fault rupture (kilometers).

The fault distance, also illustrated in Figure 6.10, is the shortest horizontal distance (measured along the earth's surface) from the lateral spread to the surface projection of the fault rupture, or zone of seismic energy release, causing the earthquake. If the site falls within the surface projection of the fault rupture, then the fault distance is zero. If the fault plane ruptures the surface of the earth, then the fault distance is measured to the nearest surface rupture.

Parameter: *Accel_max* = peak horizontal acceleration at the ground surface (g's).

This is the maximum horizontal acceleration that would occur at the surface of a site in the absence of excess pore pressures or liquefaction generated by the earthquake. Ideally, *Accel_max* would be taken from ground motions recorded at a location next to a lateral spread; however, such recordings are rarely available in the immediate vicinity of an EPOLLS case study. For some sites in the EPOLLS database, the peak acceleration was estimated from peak values recorded at stations in the area, with adjustments for distance to the earthquake source. For many EPOLLS sites, the peak acceleration was estimated by earlier investigators and included in their published site reports. The available data and published estimates of peak acceleration were also supplemented with predictions from empirical attenuation relationships. All of this information was considered in choosing an appropriate value of *Accel_max* for the EPOLLS case study sites.

Numerous empirical equations have been developed by seismologists over the years, with frequent updates as additional data are collected from recent earthquakes. Estimates from several of these equations were considered in assembling the EPOLLS database, but the values of *Accel_max* compiled generally reflect estimates from two selected empirical attenuation equations. Both equations represent the geometric mean of the orthogonal horizontal acceleration records at a site. For earthquakes in western North America, an equation given by Boore et al. (1993) was primarily used. This equation was developed for "Class C" sites (sites with soils in the upper 30 m having shear wave velocities between 180 and 360 m/s), typical of sites subject to liquefaction and lateral spreading. Using the variables defined above, the equation by Boore et al. (1993) can be written as:

$$\log(Accel\_max) = 0.229(EQ\_Mw - 6) - 0.778 \log\left(\sqrt{Fault\_Dist^2 + 5.57^2}\right) + 0.146 \qquad (6.3)$$

However, Equation 6.3 is specifically valid only for earthquakes in western North America. An attenuation equation for Japan, developed by Fukushima and Tanaka (1990), was primarily used

to estimate peak accelerations from earthquakes in the western Pacific. Again using the previously-defined EPOLLS variables, the equation given by Fukushima and Tanaka (1990) can be written as:

$$\log\left(\frac{Accel\_max}{980.66}\right) = 0.41\,EQ\_Ms - \log\left(R + 0.032 * 10^{0.41\,EQ\_Ms}\right) - 0.0034\,R + 1.30 \quad (6.4)$$

where *R* is defined as the shortest distance to the fault rupture. However, for most of the Japanese data used by Fukushima and Tanaka, the fault rupture was difficult to define and the hypocentral distance was used for *R*. Hence, in compiling *Accel_max* for the EPOLLS case studies in eastern Asia, Equation 6.4 was used with *R* = *Hypoc_Dist*.

Parameter: *Duration* = duration of strong earthquake motions (seconds).

Here, a "bracketed duration" (Kramer 1996) is used to indicate the length of time the site is subjected to strong ground motions during the earthquake. The duration is measured as the time between the first and last occurrence of a surface acceleration exceeding 0.05 g. When available, strong motion records from stations near the site of an EPOLLS case study were used to estimate the duration of shaking. When no suitable records were available, an empirical correlation proposed by Krinitzsky et al. (1988) for sites with soft soils was used:

- for plate margin earthquakes with *Focal_Depth* ≤ 19 km,

$$\log(Duration) = -2.06 + 0.43\,EQ\_Mw + 0.60\,\log(0.1\,Hypoc\_Dist) \quad (6.5)$$

- for subduction zone earthquakes with *Focal_Depth* ≥ 20 km,

$$\log(Duration) = -2.36 + 0.43\,EQ\_Mw + 0.30\,\log(0.1\,Epict\_Dist) \quad (6.6)$$

6.5. Geometrical Parameters.

In this section, the EPOLLS parameters that describe the geometry and dimensions of a lateral spread are defined. A list of the database variables in this category is also given in Table A.3.

Parameter: *Banded_Area?* = TRUE for lateral spreads of the banded-area type, FALSE if the surface area of the lateral spread is bounded on all sides.

This classification refers to the shape of the slide mass in plan. For lateral spreads with *Banded_Area?* = FALSE, a bounding line can be drawn that completely encloses the slide mass. Examples include Slide No. 9 in Figure 6.2, Slide Nos. 11 and 12 in Figure 6.3, and all of the slides in Figures 6.7 and 6.8. On the other hand, lateral spreads often occur in bands running

parallel to a stream or free face. In these "banded-area" cases (*Banded_Area?* = TRUE), horizontal displacements tend to be perpendicular to the stream and form surface fissures that are roughly parallel to the stream. While it is fairly easy to define the head and toe in lateral spreads of this type, the flanks of the slide are generally undefined. Examples of banded-area lateral spreads include Slide Nos. 8 and 10 in Figures 6.2 and 6.3.

Parameter: *Slide_Area* = surface area of the slide mass (square meters).

The slide area is the horizontal surface area of the lateral spread measured in plan view. The slide area is undefined for banded-area type lateral spreads. When both sides of a stream are subjected to extensive liquefaction and lateral spreading, the slide areas meet in the center of the stream as for the EPOLLS case studies shown in Figure 6.3.

Parameter: *Slide_Length* = length of slide area from head to toe (meters).

The slide length, as indicated in Figure 5.1, is the horizontal distance from the head of a lateral spread to the toe, measured in the prevailing direction of movement. When extensive soil liquefaction causes a lateral spread in the floodplain of a stream, the slide length is assumed to extend to the center of the stream.

Parameter: *Divergence* = divergence factor.

The divergence factor represents the change in width of the slide mass as one moves from the head toward the toe. A positive divergence factor indicates that the slide mass gets wider toward the toe, while a negative divergence factor indicates a narrowing of the slide area. Definition of the divergence factor is detailed in Figure 6.11. The divergence parameter was defined based on the hypothesis that displacements might be restrained by constriction of the flanks toward the toe, or deformations might increase if the flanks get progressively further apart.

6.6. Topographical Parameters.

This category of EPOLLS parameters includes variables representing the topography of a lateral spread, such as surface slope. These variables are listed in Table A.4 of Appendix A.

Parameter: *Direct_Slide* = direction of sliding (degrees).

The direction of sliding is measured as the angle in the horizontal plane between the prevailing direction of movement and the maximum slope. The line of maximum slope is drawn perpendicular to a free face or the principle topographical contour lines. In most lateral spreads, *Direct_Slide* is zero. In some case studies, *Direct_Slide* is greater than zero because displacements, such as the compression of a bridge, were measured in a direction that was not coincident with the maximum slope direction.

Parameter: *Free_Face?* = TRUE if free face along toe, FALSE if no free face.

A free face is any relatively abrupt, essentially vertical change in the topography along the toe of the slide. A free face in a lateral spread is most commonly a stream bank but can also be a road cut, drainage channel, etc.

Parameter: *Bulkhead?* = TRUE if flexible wall along free face, FALSE if no wall or free face.

Along a waterfront, it is not uncommon for a free face to be stabilized with an earth-retaining wall. If this wall is massive, such as the large caisson structures used in building the port facilities in Kobe, Japan, an associated liquefaction failure does not conform to the definition of a lateral spread and is not included in the EPOLLS database. However, if the wall is "flexible" (such as a steel sheet pile wall) and judged to not provide significant restraint to a large lateral spread behind the wall, the site can be used as an EPOLLS case study. The *Bulkhead?* category parameter is used to identify the EPOLLS cases studies where some type of flexible wall forms the free face but is judged to provide minimal support to a relatively large lateral spread behind the wall.

Parameter: *Face_Height* = height of free face, measured vertically from toe to crest (meters).

The face height is measured vertically from the toe to the crest of the free face, as shown in Figure 6.12. When the free face is a stream bank, the face height is measured from the submerged toe at the bottom of the stream. The height of a narrow levee at the top of a stream bank is not included in the face height. If there is no free face, *Face_Height* equals zero.

Parameter: *Top_%Slope* = average slope across the surface of the lateral spread (percent).

The surface slope is measured as the change in elevation over the horizontal distance from the head to the toe of the lateral spread, as indicated in Figure 6.12. When a free face is present, the top slope is measured from the head of the slide to the crest of the free face. Narrow levees at the tops of stream banks are ignored. Negative values of *Top_%Slope* indicate that the surface is inclined away from the direction of movement. A small negative surface slope is often found in the flood plain of a stream with a lateral spread moving toward the free face of the stream bank.

Parameter: *Eff_%Slope* = effective surface slope of the lateral spread (percent).

The effective slope is defined as the change in elevation over horizontal distance from the head of the slide to the toe of a free face, if present. This can be written in equation form as:

$$Eff\_\%Slope = Top\_\%Slope + 100.*\left(\frac{Face\_Height}{Slide\_Length}\right) \qquad (6.7)$$

The effective surface slope combines the effects of face height and top surface slope into a single variable. In an idealized sense, the effective slope represents the static stress driving the lateral spread.

Parameter: *Bot_%Slope* = average slope along the bottom of the liquefied deposit (percent).

The bottom slope is measured as the change in elevation over the horizontal distance along the bottom of the liquefied soil deposit underlying a lateral spread, as illustrated in Figure 6.12. Like the top slope, a negative bottom slope indicates a slope in a direction opposite to the prevailing direction of movement. While this variable is classified as a topographical parameter in EPOLLS, evaluation of the subsurface soil conditions is required to define *Bot_%Slope*.

6.7. Geotechnical Parameters.

The geotechnical parameters in the EPOLLS database represent the soil conditions underlying a lateral spread. Based on an analysis of available geotechnical soil borings, the EPOLLS geotechnical parameters indicate the:

- thickness of liquefied soil,
- average shear resistance of the liquefied soil,
- minimum shear resistance in the liquefied soil,
- gradation of the liquefied soil, and
- strength and permeability of unliquefied soil above and below the liquefied soil.

Thirty-eight geotechnical parameters, discussed in this section and listed in Table A.5, were defined for the EPOLLS database. To compile these parameters for 59 EPOLLS case studies, 248 soil borings were analyzed. A computer program was written to process this data and compute the EPOLLS geotechnical parameters. Called "EPOLIQAN", for *EPOLLS LIQuefaction ANalysis*, this computer code is documented in Appendix C.

The EPOLLS geotechnical parameters are computed from the logs of soil borings with Standard Penetration Tests (SPTs). First, the measured SPT blowcounts (blows per foot) are converted to a normalized, corrected value labeled as $(N_1)_{60}$. Based on the $(N_1)_{60}$ value, the liquefaction resistance of the soil is calculated along with the cyclic stress induced by the earthquake at the same depth. The factor of safety against liquefaction (FS_{liq}) is then computed for every SPT depth in the boring. A $FS_{liq} \leq 1.0$ is interpreted to mean the soil liquefied at that depth during the earthquake. The vertical profile of FS_{liq} thus indicates the liquefied soil thickness at each boring location. The empirical procedure used to analyze the soil boring data and compute the factor of safety profile is discussed fully in Chapter 7. The geotechnical parameters discussed here are all based on values of $(N_1)_{60}$, factor of safety against liquefaction, and the liquefied thickness in the soil borings at the EPOLLS case study sites.

When Standard Penetration Tests are performed in a soil boring, the tests are typically conducted at depth intervals of one to two meters. The $(N_1)_{60}$ value and factor of safety against liquefaction can be computed only at these discrete testing depths in the boring log. In addition, because the grain size distribution is usually determined from laboratory analysis of the SPT samples, the soil gradation is often available only for these testing depths. Consequently, all of

the EPOLLS geotechnical parameters are computed directly or indirectly from data at the SPT locations. For some parameters, an average value is calculated from data at all SPT locations in the liquefied thickness. For example, the parameter *FS_Min* is the single minimum factor of safety determined at the depth of an SPT. On the other hand, the parameter *FS_Liq* is the average factor of safety in the liquefied thickness; that is, the factor of safety determined from each SPT in the liquefied thickness is averaged to give *FS_Liq*. Similarly, the parameter *Fine_Liq* is an average of the fines content measured at all depths in the liquefied thickness.

The depth to the top and bottom, as well as the thickness, of liquefied soil are also computed from the SPT values in the soil boring logs. However, the boundaries between liquefied and unliquefied soil usually fall between SPT depths. Thus, to estimate the liquefied thickness in a boring log, a continuous, interpolated profile is needed. The procedure used to compute the interpolated profile (to 0.1 m depth increments) in the EPOLIQAN program is discussed in Section 7.5. In some cases, however, the computed, interpolated profile is not a good representation of the field conditions. For example, the EPOLIQAN code may indicate an unliquefied sand seam in the middle of a much thicker liquefied deposit. While this is possible, it is usually reasonable to assume such a seam will liquefy due to pore pressure migration. Hence, to allow for interpretations based on engineering judgment, the liquefied thickness can be specified by the user of the EPOLIQAN code (see Appendix C).

A summary of these considerations in the calculation of the EPOLLS geotechnical parameters is presented in Table 6.1. In the middle two columns, calculation of the parameters using only data from the SPT depths or the interpolated continuous soil profile is indicated. Some of the EPOLLS parameters are values from the SPT depths averaged over the liquefied thickness, which is either predicted from the interpolated profile or specified. In the EPOLIQAN code, these parameters are actually computed twice: once using the predicted liquefied thickness, and a second time using the specified liquefied thickness. The EPOLLS parameters that depend on the liquefied thickness are indicated by the entry in the last column of Table 6.1.

In addition, while a soil boring measures the soil conditions at one specific location, the geotechnical parameters in the EPOLLS database must represent the subsurface conditions across the entire area of a lateral spread. To represent the soil conditions across a lateral spread, data from all of the available soil borings are used to define the appropriate EPOLLS parameters. Hence, in the EPOLLS database, two values of each geotechnical parameter are listed: an *Avg-* parameter representing the average value across the site, and a *Rng-* parameter representing the range (maximum minus minimum values) across the site. For example, the parameter *Avg-Z_GrWater* represents the average depth to ground water, while *Rng-Z_GrWater* is the difference between the maximum and minimum depth to ground water across the site. Whether data is available from one or multiple soil borings, the *Avg-* and *Rng-* values are estimated from all available information. In particular, the *Avg-* and *Rng-* values of the liquefied thickness are best estimated from the general engineering knowledge of the subsurface geology at the site. In

compiling the EPOLLS database, all available subsurface information was used, including data from in situ penetration tests other than SPT's. While the definition of *Avg-* and *Rng-* parameters is fairly subjective, this approach allows the engineer to use all available data to describe the subsurface soil conditions.

Nineteen EPOLLS geotechnical parameters are defined in the list that follows. For each, an *Avg-* and *Rng-* value is compiled in the database for a maximum of 38 entries describing the soil conditions beneath a lateral spread.

Parameter: *Z_GrWater* = depth to ground water (meters).

This is the depth to the static ground water table, measured vertically from the surface.

Parameter: *Z_TopLiq* = depth to top of liquefied soil (meters).

This depth is measured from the surface to the top of the shallowest liquefied soil sublayer. *Z_TopLiq* is equal to the thickness of the unliquefied soil above the liquefied zone. For many lateral spreads, the top of the liquefied soil coincides with the ground water table.

Parameter: *Z_BotLiq* = depth to bottom of liquefied soil (meters).

This depth is measured to the bottom of the deepest liquefied soil sublayer. In EPOLIQAN, the predicted value of *Z_BotLiq* does not exceed the maximum depth in a soil boring. When liquefaction is predicted at the very bottom of a soil boring, data from deeper penetration tests are needed to establish the correct value of *Z_BotLiq.*

Parameter: *Thick_Liq* = thickness of liquefied soil (meters).

The vertical thickness of liquefied soil can be defined in one of two general ways, as depicted in Figure 6.13. The liquefied thickness (*Thick_Liq*) can be defined as the gross liquefied thickness (equal to *Z_BotLiq* minus *Z_TopLiq*) or as the summation of the liquefied sublayer thicknesses. When only one soil layer liquefies, both definitions yield the same value of *Thick_Liq.* However, when more than one liquefied layer is expected, these two definitions can give significantly different values. The choice between the two definitions for *Thick_Liq* is subjective and left to the judgment of the engineer. This choice should be made so that *Thick_Liq* best represents the thickness of soil experiencing significant loss of shear strength in a lateral spread. The following guidelines are suggested:

- If a major soil unit liquefies, with the possibility of thin, unliquefied seams, use the gross liquefied thickness for *Thick_Liq.*
- If liquefaction occurs in thin sublayers of the soil profile, use the summation of the liquefied thicknesses for *Thick_Liq.*

This distinction is further illustrated in Figure 6.13. For most of the EPOLLS cases studies, liquefaction occurred throughout most of a major soil unit and the gross liquefied thickness was used.

Parameter: *Index_Liq* = index of liquefied thickness in the upper 20 meters.

This parameter represents the net shear resistance of the soil profile, with more weight given to the soil strength at shallower depths. The *Index_Liq* is based on a weighted index proposed by Hamada et al. (1986) and computed over the upper 20 m of the soil profile. However, the index given by Hamada and his colleagues is not consistently defined for a soil boring that does not extend to a depth of 20 m. With this in mind, the weighted index proposed by Hamada et al. (1986) was normalized for the maximum depth of the soil boring to give the EPOLLS parameter *Index_Liq*:

$$Index\_Liq = \frac{\sum_{z=0}^{z_{bot}} F \cdot W \cdot \Delta z}{\sum_{z=0}^{z_{bot}} W \cdot \Delta z} \qquad (6.8)$$

Here, z is the depth in meters, z_{bot} is the maximum depth (not exceeding 20 m) where FS_{liq} is determined, and Δz is the depth increment to which FS_{liq} is interpolated (Δz = 0.1 m in the EPOLIQAN code). At depths where liquefaction is predicted ($FS_{liq} \leq 1.0$), the strength function is $F = 1.0 - FS_{liq}$. At depths where $FS_{liq} > 1.0$ or in soils otherwise not subject to liquefaction, the strength function is F = 0.0. The weight function (W), which varies linearly from 10.0 at the ground surface to 0.0 at a depth of 20 m, is the same as defined by Hamada et al. (1986): W = 10.0 - 0.5z. Theoretically, the index of liquefied thickness (*Index_Liq*) varies from 0.0 to 1.0. If no liquefaction occurs ($FS_{liq} > 1$, F=0) throughout the soil profile down to 20 m, then *Index_Liq* is 0.0. Values of *Index_Liq* close to 1.0 indicate severe liquefaction.

Parameter: *FS_Liq* = average factor of safety in the liquefied soil thickness.

The factor of safety against liquefaction (FS_{liq}), as defined in Section 7.5, is the cyclic resistance ratio of the soil divided by the cyclic stress ratio induced by the earthquake. The parameter *FS_Liq* is the average value of FS_{liq} determined from all of the Standard Penetration Tests in the liquefied thickness. The FS_{liq} values at each SPT location are not altered when the liquefied thickness is specified in the EPOLIQAN code, although this does affect which FS_{liq} values are averaged to get *FS_Liq*.

Parameter: *N160_Liq* = average $(N_1)_{60}$ measured in the liquefied thickness (blows per foot).

The $(N_1)_{60}$ value is the SPT blowcount corrected for a standard 60% energy level and normalized with respect to the overburden stress. The corrections used to compute $(N_1)_{60}$ are detailed in Chapter 7.

Parameter: *FS_Min* = minimum factor of safety measured in potentially liquefiable soil.

This is the lowest factor of safety against liquefaction determined from a Standard Penetration Test. Low values measured in soils not subject to liquefaction, such as unsaturated

or clayey soils, are excluded. This value represents the lowest shear resistance measured in a liquefiable soil in a soil boring.

Parameter: *N160_MnFS* = measured $(N_1)_{60}$ corresponding to *FS_Min* (blows per foot).

The corrected SPT blowcount indicating the minimum factor of safety against liquefaction, this parameter is another measure of the minimum shear resistance.

Parameter: *Z_MnFS* = depth corresponding to *FS_Min* (meters).

This is the depth of the SPT blowcount indicating the minimum factor of safety. If two or more values of *FS_Min* are equal in one boring, use the depth to the shallowest value.

Parameter: *N160_Min* = lowest $(N_1)_{60}$ measured in a potentially liquefiable soil (blows per foot).

The lowest corrected SPT blowcount $(N_1)_{60}$ is used as an alternative indication of the weakest sublayer in the soil column. Low values in soils not subjected to liquefaction are excluded.

Parameter: *Z_MnN160* = depth corresponding to *N160_Min* (meters).

This is the depth to the SPT yielding the lowest measured $(N_1)_{60}$ value. If two or more values of *N160_Min* are equal in one boring, use the depth to the shallowest value.

Parameter: *D50_Liq* = average of mean grain size in the liquefied soil thickness (millimeters).

The mean grain size (D_{50}) is the sieve opening size through which half of the soil grains will pass. This parameter gives as indication of the coarseness of the soil grains in the liquefied soil deposit.

Parameter: *Cu_Liq* = average coefficient of uniformity in the liquefied soil thickness.

The coefficient of uniformity (C_u) is defined as the D_{60} size (60% of the soil grains are smaller than D_{60}) divided by the D_{10} size (10% of the grains are smaller). This parameter indicates the range in grain sizes present in the liquefied soil deposit.

Parameter: *Clay_Liq* = average clay content in the liquefied soil thickness (percent).

Here, clay content is defined as the percent by weight finer than 0.005 mm.

Parameter: *Fine_Liq* = average fines content in the liquefied soil thickness (percent).

The fines content is defined as the percent by weight finer than 0.075 mm (passes a No. 200 sieve). In addition to possibly indicating the strength and stiffness of the liquefiable soil, this parameter is an indicator of how quickly excess pore pressures can drain through the liquefied deposit.

Parameter: *N160_Cap* = average $(N_1)_{60}$ measured above *Z_TopLiq* (blows per foot).

This parameter represents the average strength of the intact, surficial soil (the "cap" layer) above the liquefied deposit.

Parameter: *Fine_Cap* = average fines content in deposit above the liquefied soil (percent).

To compute this parameter, the fines content (percent finer by weight than 0.075 mm) measured at depths less than *Z_TopLiq* are averaged. However, only the fines content in the same stratum as *Z_TopLiq* and one stratum above are included in this average. This parameter represents the permeability of soils above the liquefied soil and indicates how quickly excess pore pressures can drain upward.

Parameter: *Fine_Base* = average fines content in deposit below the liquefied soil (percent).

Here, the fines content (percent finer by weight than 0.075 mm) measured at depths greater than *Z_BotLiq* are averaged. However, values measured in soil strata deeper than one stratum below the liquefied soil deposit are not used in this average. This parameter represents the permeability of soils below the liquefied soil and indicates how quickly excess pore pressures can drain downward.

Table 6.1. Calculation of the EPOLLS geotechnical parameters based on SPT blowcounts and the liquefied thickness in one soil boring.

EPOLLS Parameter	Values computed using:		Value depends on liquefied thickness (predicted or specified)
	Data at SPT Depths	Interpolated Soil Profile	
Z_TopLiq		✓	Yes
Z_BotLiq		✓	Yes
Thick_Liq		✓	Yes
Index_Liq		✓	No
FS_Liq	✓		Yes
N160_Liq	✓		Yes
FS_Min	✓		No
N160_MnFS	✓		No
Z_MnFS	✓		No
N160_Min	✓		No
Z_MnN160	✓		No
D50_Liq	✓		Yes
Cu_Liq	✓		Yes
Clay_Liq	✓		Yes
Fine_Liq	✓		Yes
N160_Cap	✓		Yes
Fine_Cap	✓		Yes
Fine_Base	✓		Yes

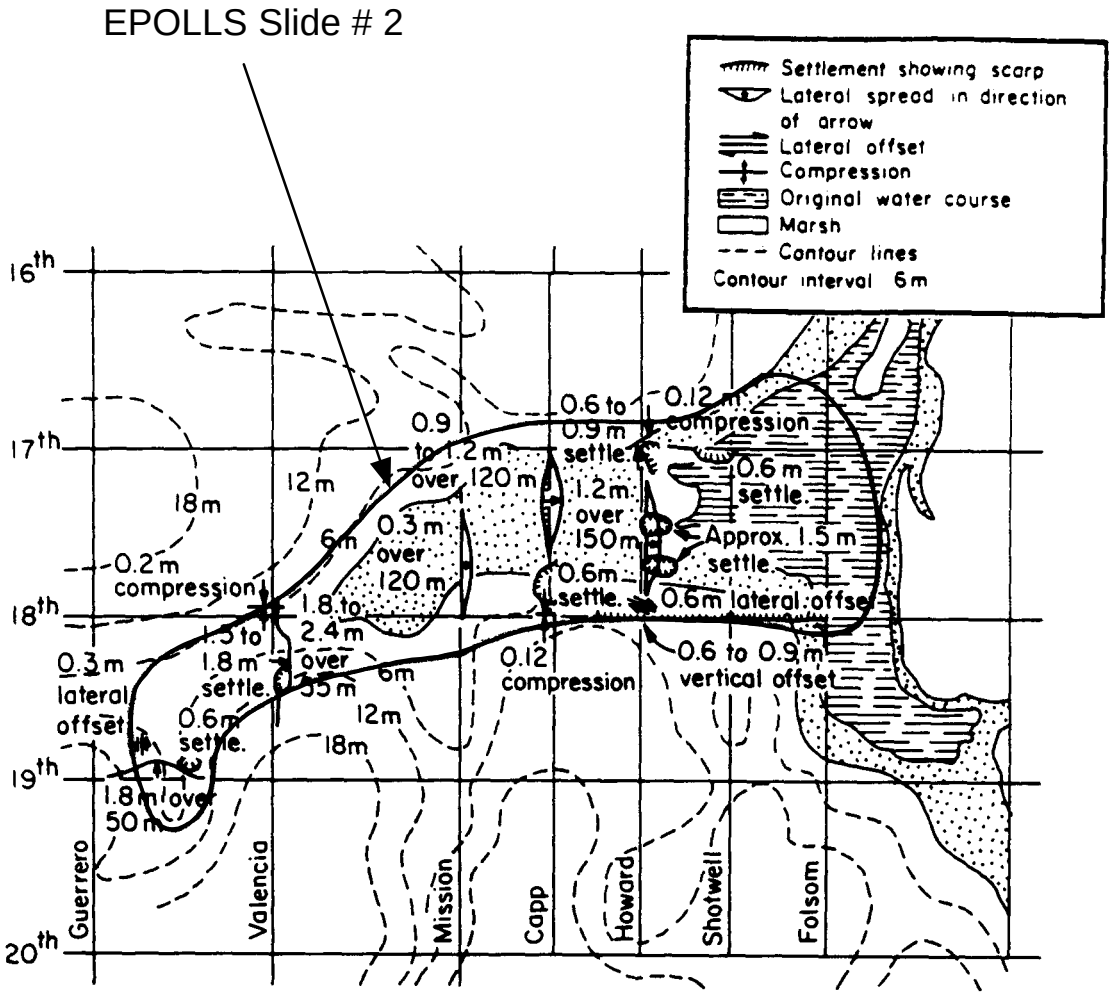

Figure 6.1. EPOLLS case study in San Francisco, California, caused by the 1906 earthquake (base map from O'Rourke et al. 1992a).

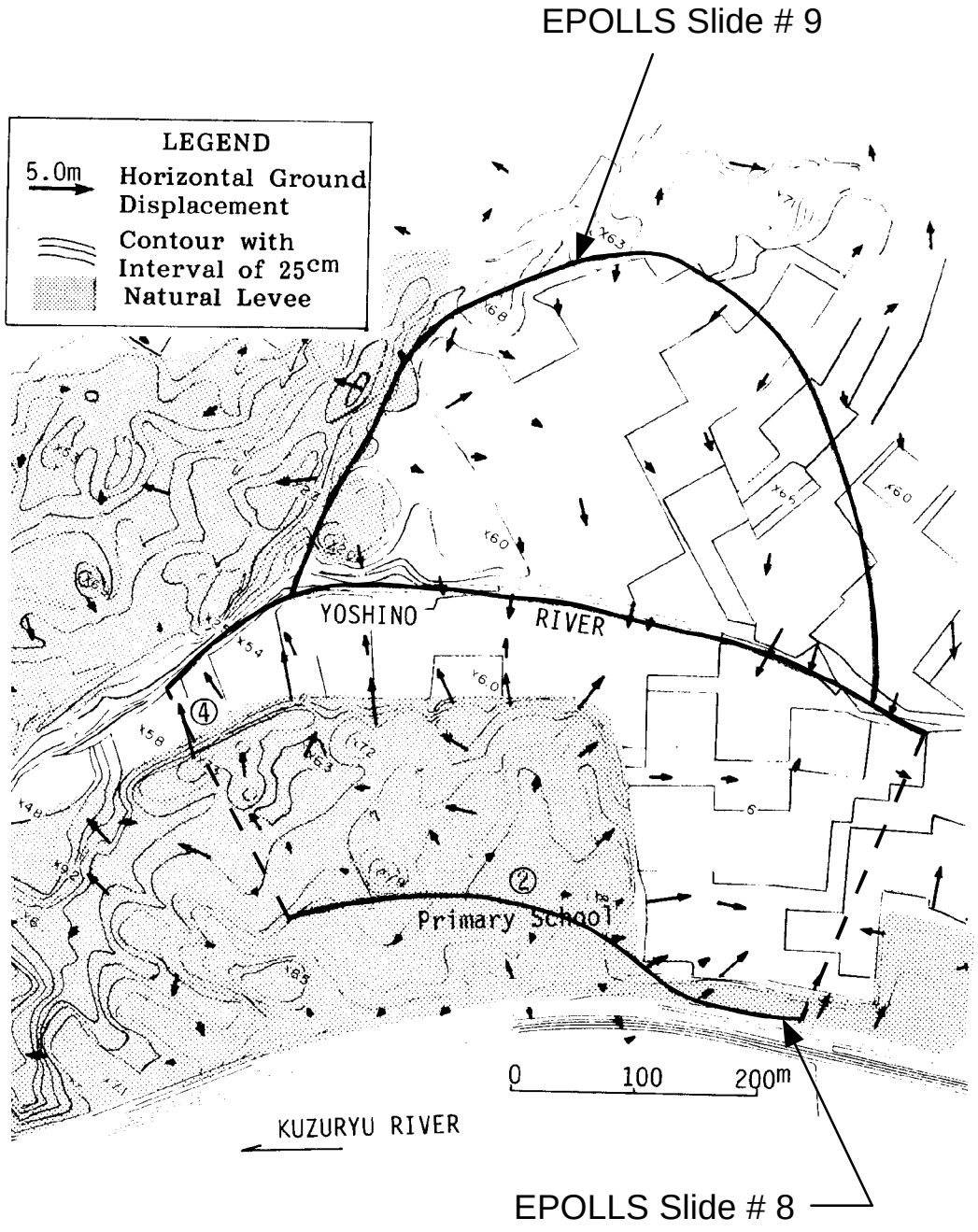

Figure 6.2. EPOLLS case studies caused by the 1948 Fukui, Japan, Earthquake (base map from Hamada et al. 1992).

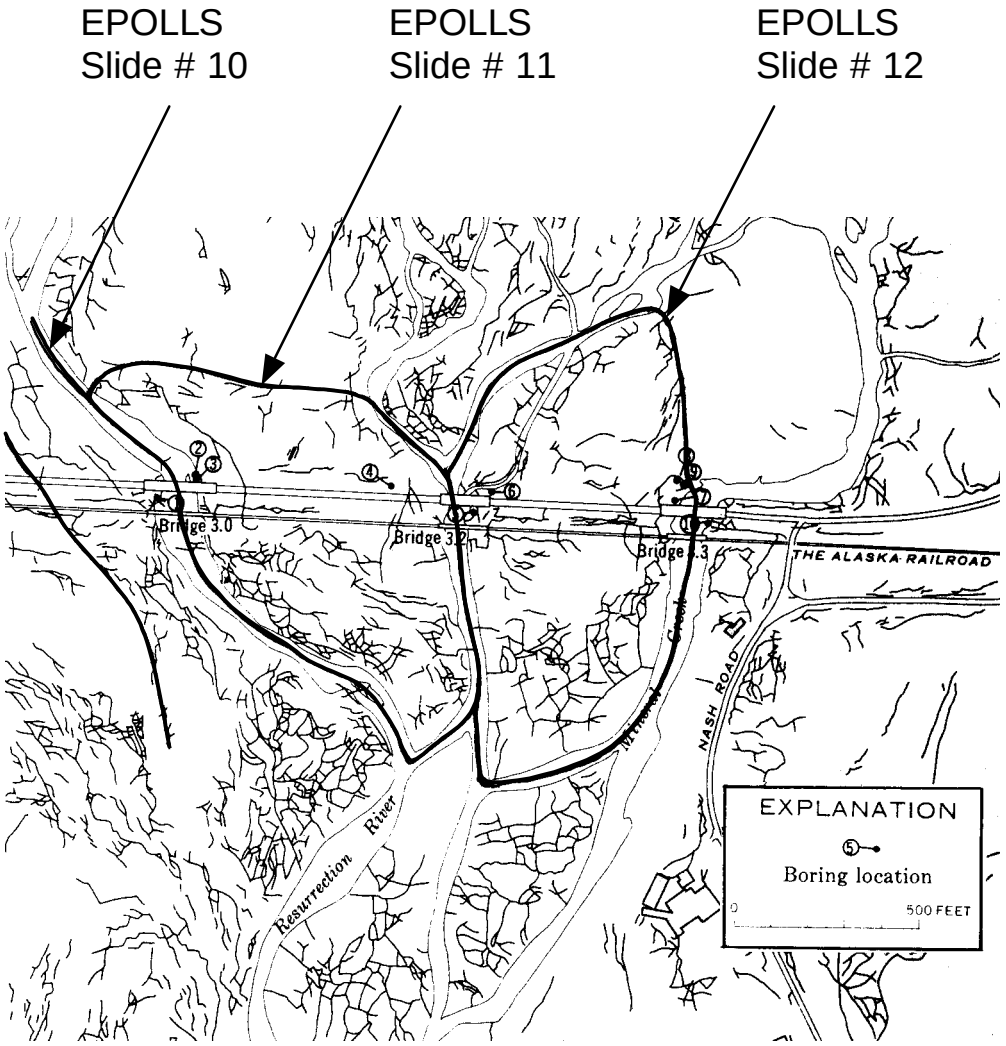

Figure 6.3. EPOLLS case studies along the Alaska Railroad caused by the 1964 Prince William Sound Earthquake (base map from McCulloch and Bonilla 1970).

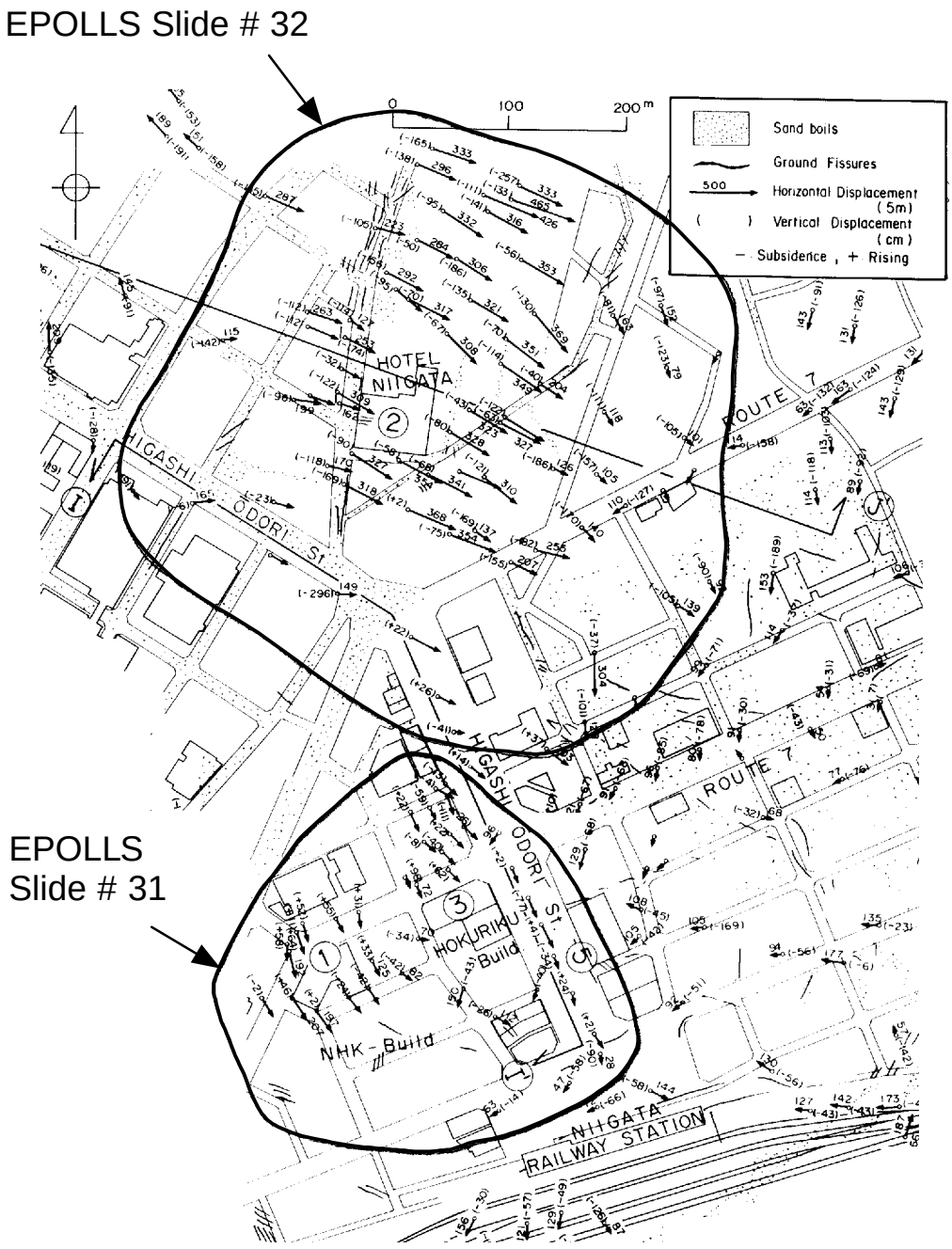

Figure 6.4. EPOLLS case studies in Niigata, Japan, caused by the 1964 earthquake (base map from Hamada 1992a).

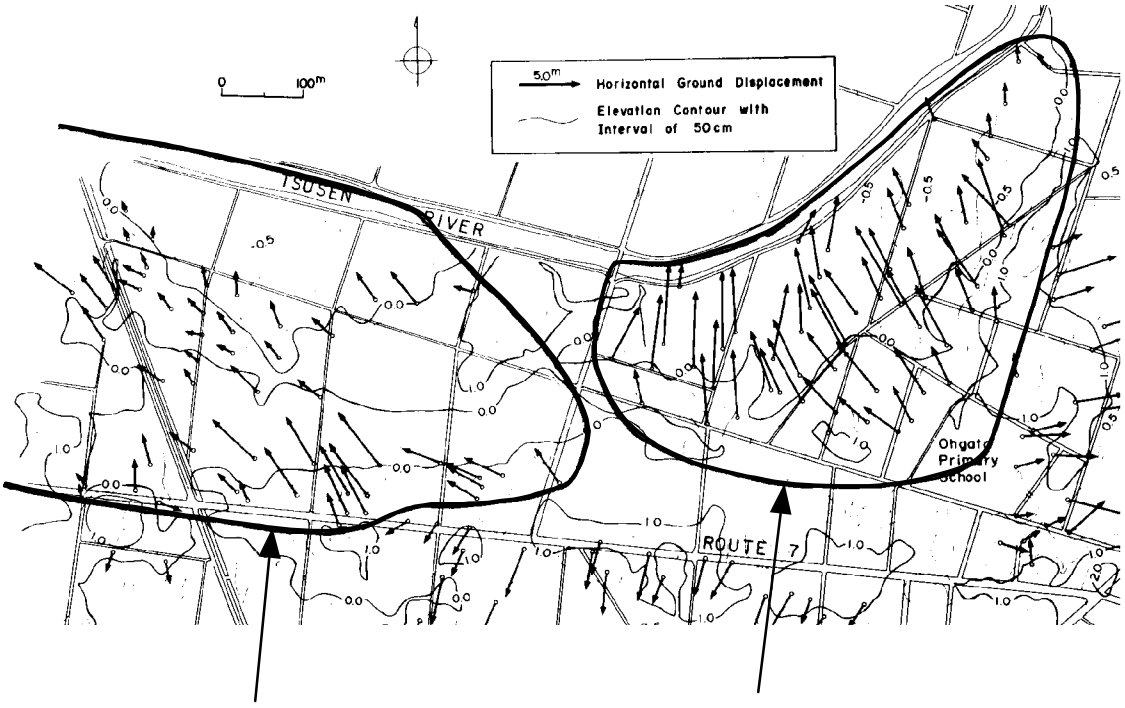

Figure 6.5. EPOLLS case studies east of Niigata, Japan, caused by the 1964 earthquake (base map from Hamada 1992a).

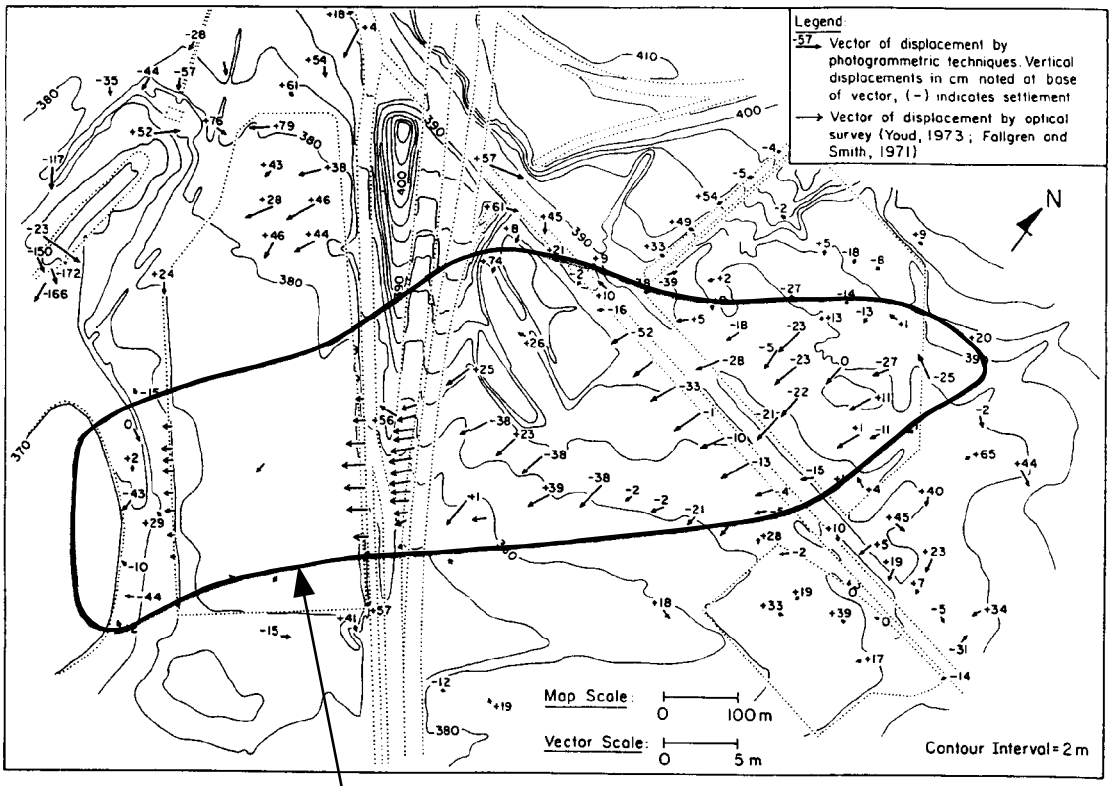

Figure 6.6. EPOLLS case study in San Fernando, California, caused by the 1971 earthquake (base map from O'Rourke et al. 1992b).

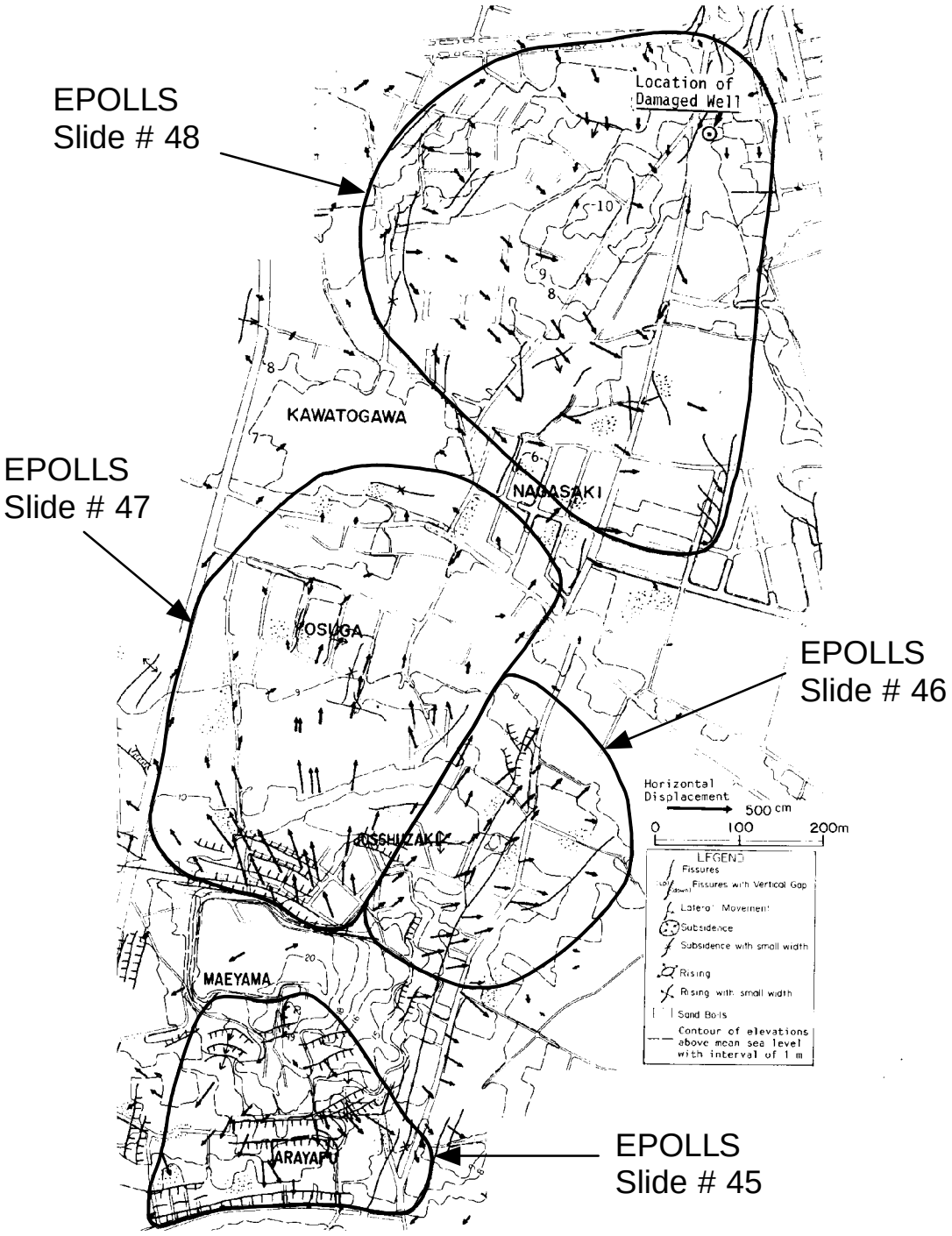

Figure 6.7. EPOLLS case studies in Noshiro, Japan, caused by the 1983 Nihonkai-Chubu Earthquake (base map from Hamada 1992b).

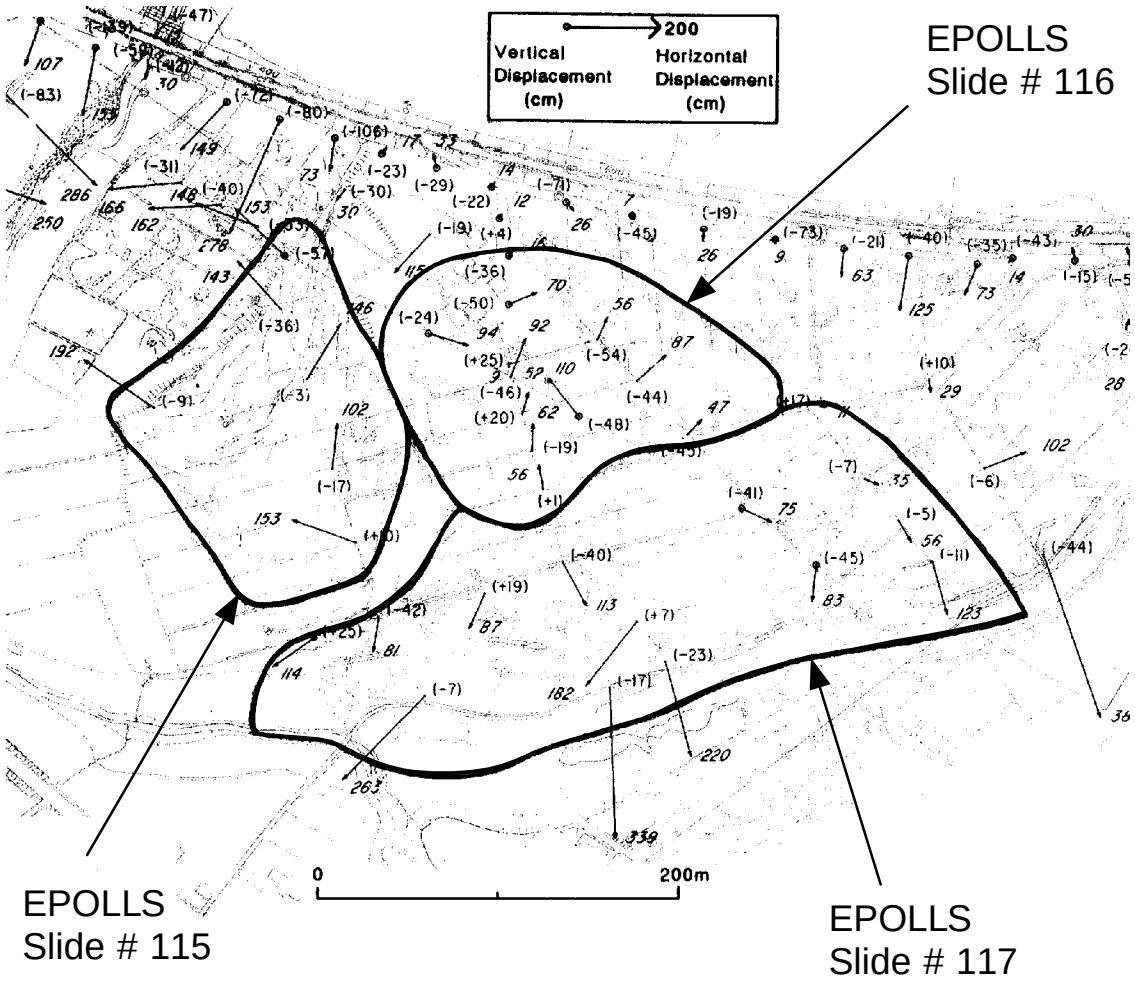

Figure 6.8. EPOLLS case studies along the Shiribeshi-toshibetsu River caused by the 1993 Hokkaido Nansei-oki Earthquake (base map from Isoyama 1994).

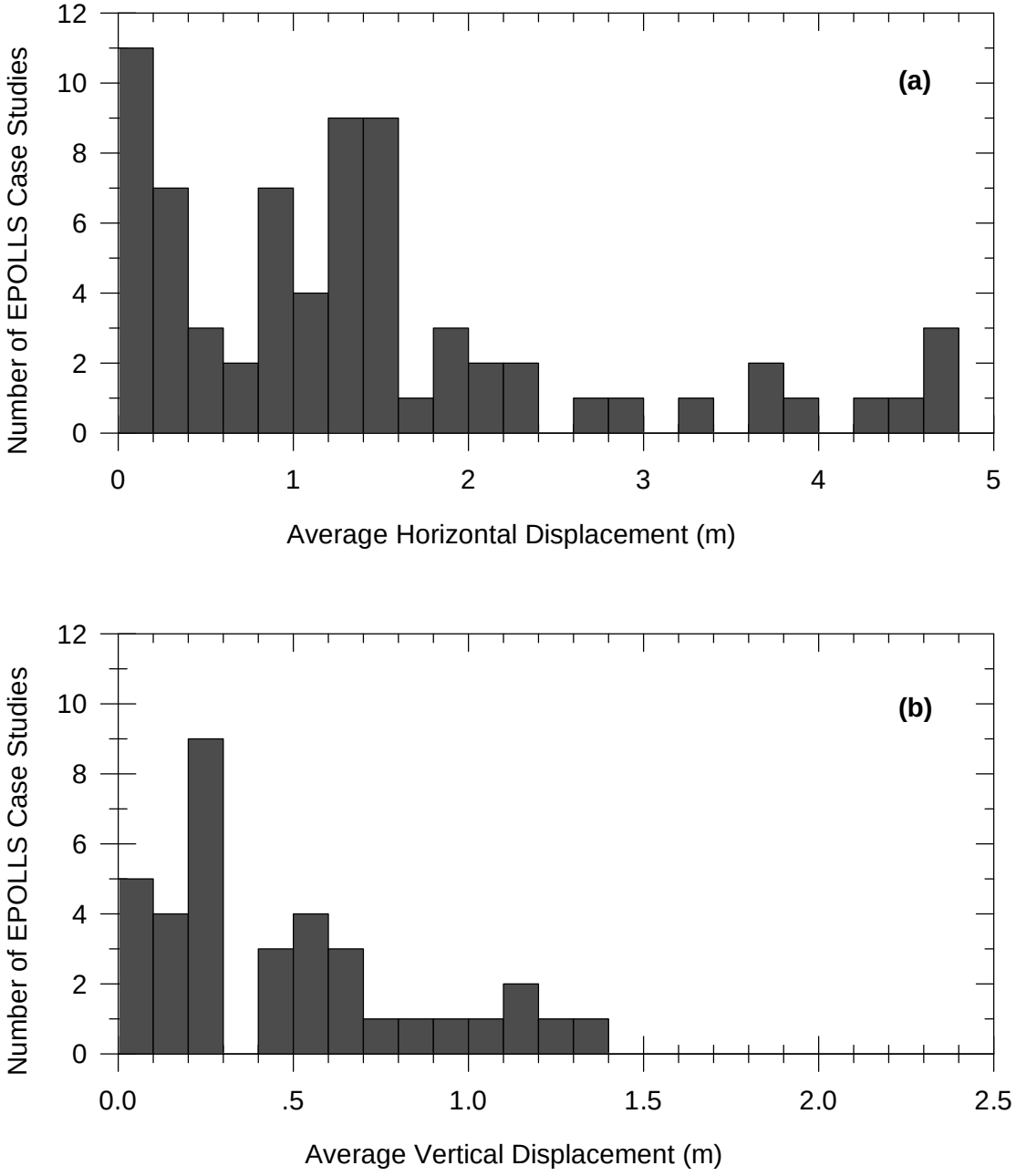

Figure 6.9. Histograms of average (a) horizontal and (b) vertical displacements in lateral spread case studies compiled in the EPOLLS database.

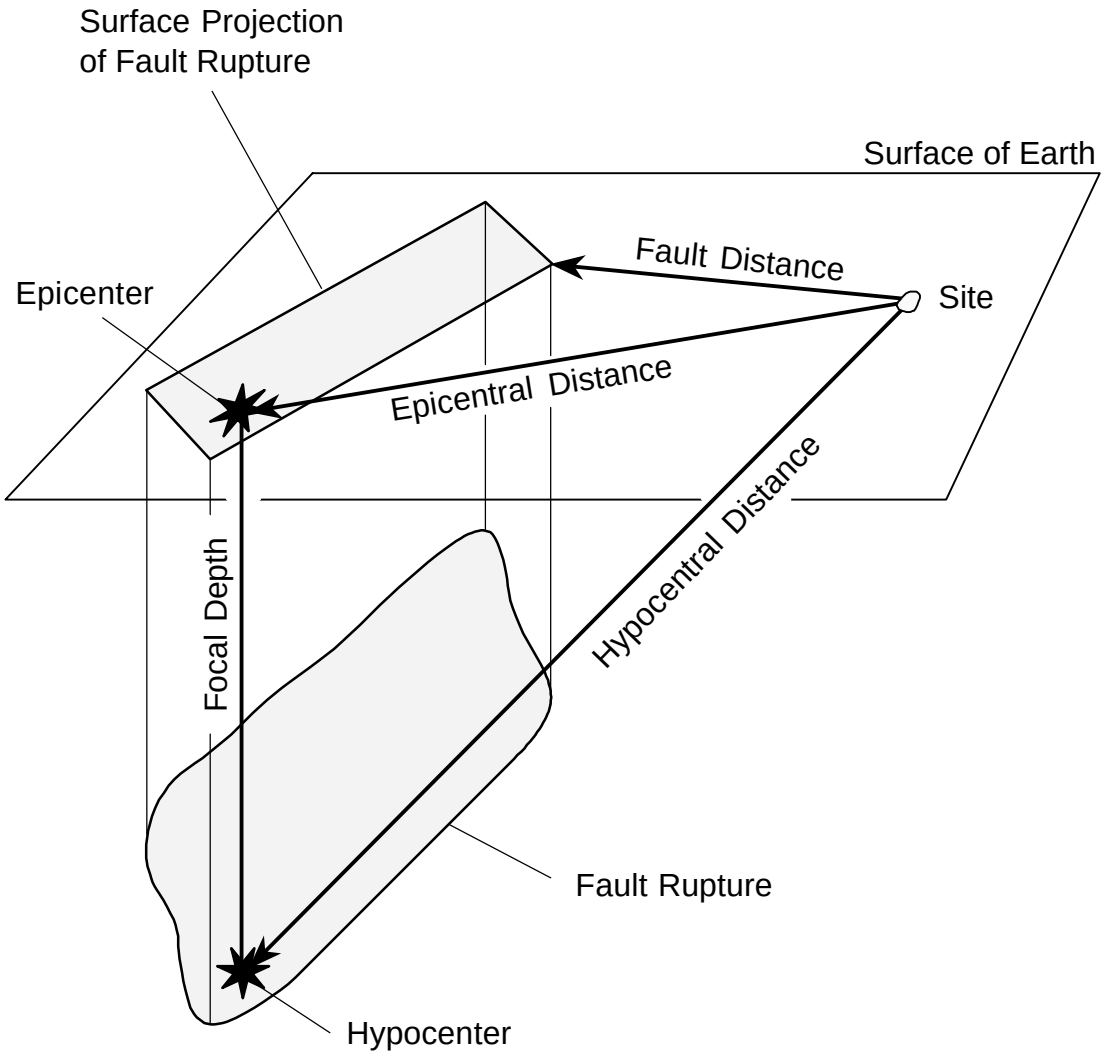

Figure 6.10. Definitions of distance to earthquake source used in the EPOLLS database.

Steps in determining the *Divergence* parameter:

(1) Draw reference line A-A in the middle of the slide mass in the prevailing direction of movement. Measure the length of this line (*L*).
(2) Find the midpoint of the reference line A-A, half-way between the head and toe of the slide.
(3) Measuring perpendicularly from the midpoint of the reference line A-A, locate the points marked ☆. If the flank of the lateral spread is less than *L/2* from the reference line, place ☆ on the boundary of the slide mass.
(4) Draw two lines, B-B and C-C, through ☆ on each flank. These lines should parallel the flanks of the slide and/or follow the dominate displacement direction in this area.
(5) At the ends of the reference line A-A, measure the perpendicular distance between B-B and C-C at the head (W_{top}) and toe (W_{bot}).
(6) Compute the divergence factor:

$$Divergence = \frac{W_{bot} - W_{top}}{L}$$

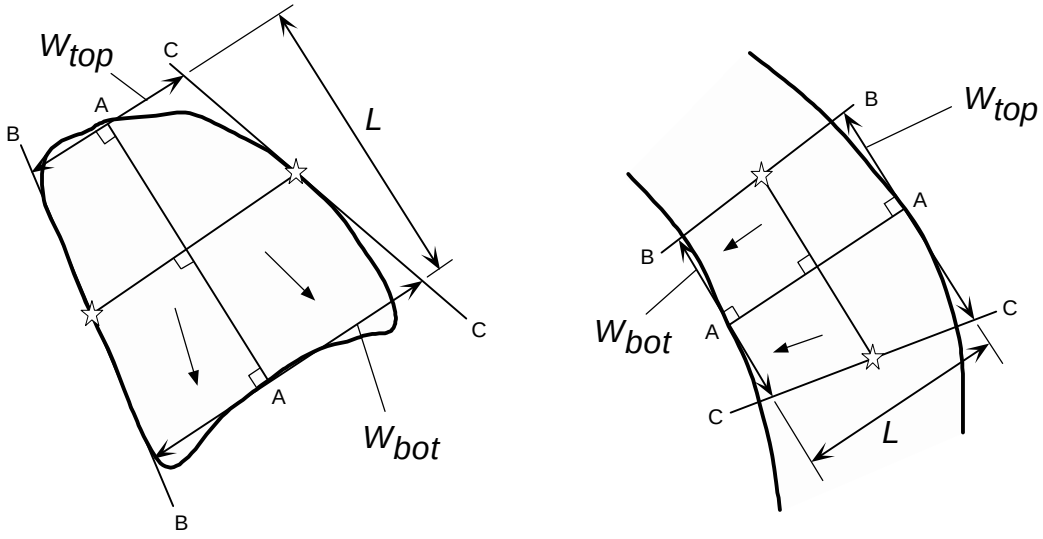

Figure 6.11. Definition of the *Divergence* parameter in the EPOLLS database.

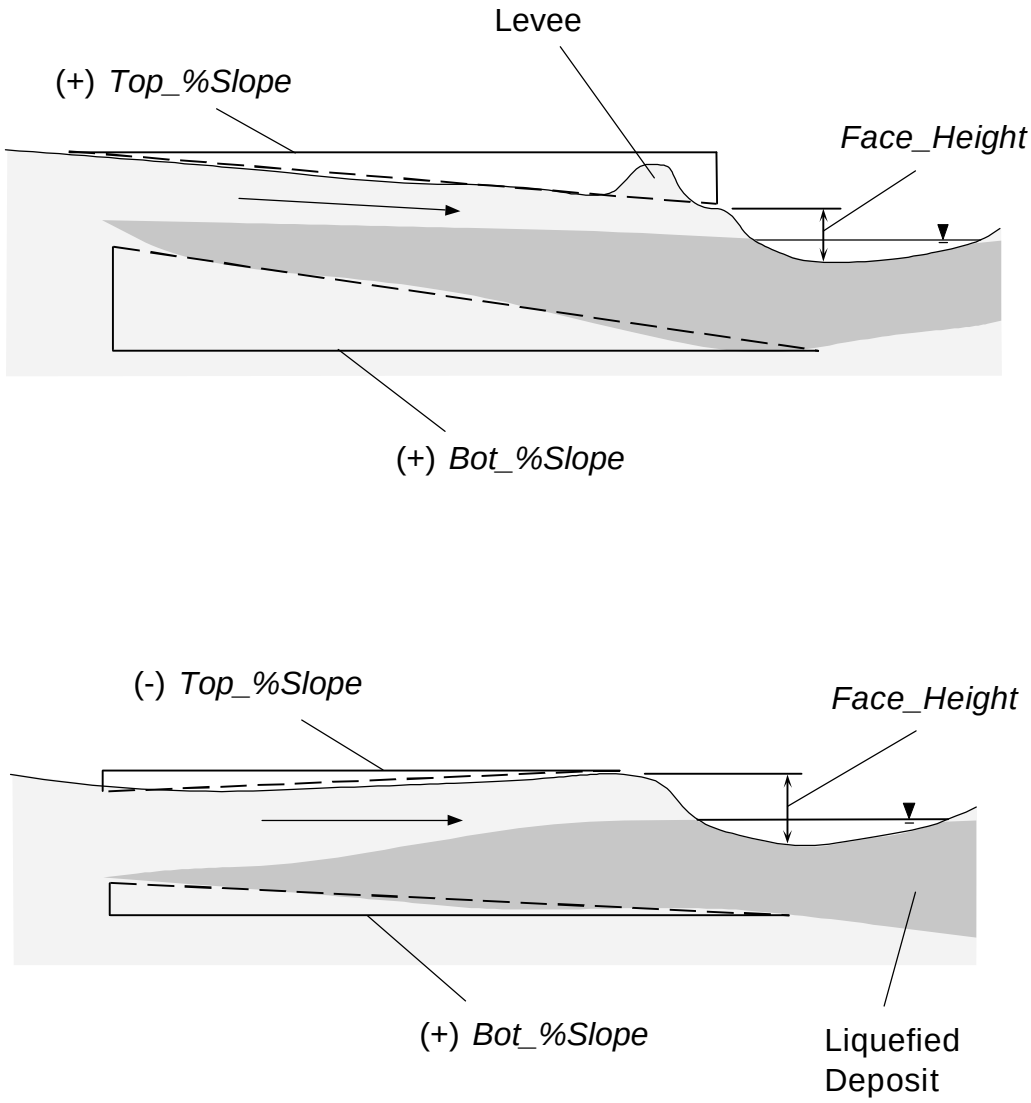

Figure 6.12. Definition of EPOLLS parameters from the topography of a lateral spread.

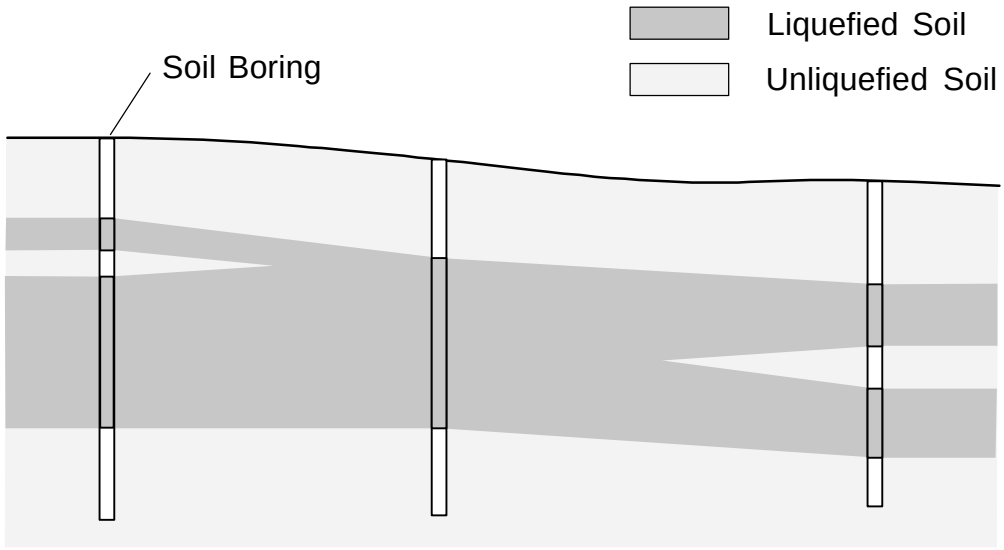

Liquefied soil deposit with unliquefied seams:

- Use the **gross** liquefied thickness
- *Thick_Liq* = *Z_BotLiq* - *Z_TopLiq*

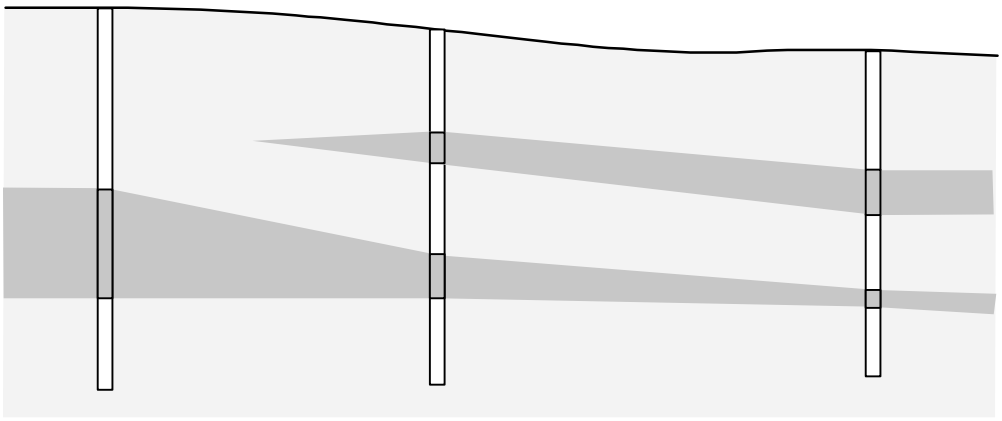

Liquefied soil in relatively thin sublayers:

- Use the **summation** of liquefied thicknesses
- *Thick_Liq* = Σ thickness of liquefied sublayers

Figure 6.13. Definition of liquefied thickness for EPOLLS when more than one sublayer liquefies.